Microfluidic Platform for Magnetic Nanoparticle Trapping and Detection

Charles A. E. Little[1,2], John Pellegrino[1], and Stephen E. Russek[2]

[1]Mechanical Engineering Department, University of Colorado, Boulder, CO 80309 USA
[2]National Institute of Standards and Technology, Boulder, CO 80305 USA

We evaluate giant magnetoresistance sensors to trap and count small concentrations of magnetic nanoparticles (MNPs) within microfluidic flow. The device presented takes the novel approach of capturing and detecting MNPs utilizing the strong fringe-fields present on the periphery of the patterned sensor. The presence of MNPs manifests as a field shift in the magnetoresistance curve. Tests of the device have shown a noticeable response to MNPs with 30 nm nominal core diameters at concentrations as low as $1.2 \times 10^{10} \pm 4.0 \times 10^{9}$ MNP/mL at a flow rate of 5 μL/min. Such a device would be beneficial for bio-medical applications, including immunoassays, and for monitoring filtration processes, where large sample fluid volumes and low MNP concentration sensitivities are required.

***Index Terms*—Giant magnetoresistance, magnetic particles, magnetic sensors, microfluidics.**

I. Introduction

GIANT MAGNETORESISTANCE (GMR) is a phenomenon that occurs in thin-film magnetic materials, where each layer's thickness is on the order of a few nanometers. The electrical resistance of such materials changes due to the presence of magnetic fields, where the maximum magnetoresistance (MR) $((\mathrm{R_{max}} - \mathrm{R_{min}})/\mathrm{R_{min}})$ is between 5% and 100% [1]. GMR materials are thus well-suited for use as micromagnetic sensors. Spin-valves (SVs) are a specific category of GMR material that rely on two magnetic layers, a *free layer* and a *pinned layer*, separated by a nonmagnetic *spacing layer*. SV sensors have found many applications, including read heads in magnetic hard drives and as industrial magnetic sensors.

GMR sensors hold promise for a number of bio-medical applications; they provide high sensitivity and high-bandwidth response in the presence of magnetic particle/labels, when compared with the traditional use of enzymes, radioisotopes or fluorescent tagging. A large body of research has already investigated the use of GMR sensor arrays for counting bio-molecules and quantifying bio-molecular interactions (GMR assays). The first GMR assay of its kind was created by Baselt *et al.* in 1998 [2].

Previous GMR assay research has looked both at detecting magnetic beads (with diameters greater then 300 nm) and magnetic nanoparticles (MNPs) (with diameters less than 100 nm). GMR arrays have proved highly sensitive to the presence of single magnetic beads. Due to their decreased magnetic volume, compared to magnetic beads, MNPs have a relatively small magnetic moment, making them difficult to detect. However, many bio-medical applications would benefit from the use of MNPs, rather than magnetic beads; Decreasing the size of the magnetic particles would have the effect of increasing the sensitivity of GMR assays to analyte concentrations. Similarly, membrane integrity testing, with MNPs, would be preferable for probing nanofiltration membranes.

Manuscript received October 31, 2012; revised February 03, 2013 and February 19, 2013; accepted February 27, 2013. Date of current version July 15, 2013. Corresponding author: C. A. E. Little (e-mail: charles.little@colorado.edu).

Color versions of one or more of the figures in this paper are available online at http://ieeexplore.ieee.org.

Digital Object Identifier 10.1109/TMAG.2013.2251416

GMR sensors have successfully detected concentrations of MNPs with 16 nm nominal core diameters to a resolution of ~23 particles [3]. The drop-dry technique used to deliver magnetic particles to the surface of the GMR sensor array, however, restricts the amount of liquid that can be probed, making such sensors impractical for industrial deployment. The solution has been to array GMR sensors in conjunction with microfluidic channels, to thereby increase the sensing area in contact with suspensions of magnetic beads by restricting the suspension fluid to a region near the detection volume of the sensors. Work by Altman *et al.* [4], based on earlier work by Mirowski *et al.* [5], and work by Millen *et al.* [6], showed that magnetic beads $\sim 1\ \mu\mathrm{m}$ in diameter can be detected in a constant microfluidic flow environment using GMR sensors. For MNPs however, microfluidic channels alone do not bring particles close enough to the sensors for adequate detection. All previous GMR sensors have detected the presence of magnetic particles by proximity to the surface of the SV elements. Altman's unique approach utilized the intrinsic fringe-fields produced on the periphery of patterned SV elements to pull in and trap magnetic beads to the edge of the sensor. Captured beads cause a detectable change in the MR response curve. In this paper, we present proof-of-concept research on the use of fringe-field capture and detection as applied to MNPs, thereby allowing for MNP detection within microfluidic flow. An illustration of MNP fringe-field trapping can be seen in Fig. 1.

In Altman's work, captured beads are detected as an increase in switching field [4]. Because the beads are on the same order of size as the SV, they cause a noticeable change to the switching dynamics of the SV. MNPs have a considerably smaller effect on the SV compared to magnetic beads. Our hypothesis is that, when captured on the periphery of the patterned SVs, MNPs should effectively increase magnetostatic coupling between layers, manifesting as a field shift in the SV's MR curve.

II. Materials and Methods

A. SV Recipe

The SV stack was deposited by use of DC magnetron sputtering on ⟨100⟩ 3-inch silicon wafers, with silicon thermal oxide. The optimized SV stack, starting from the substrate, consists of $\mathrm{Ta}(5.0)/\mathrm{Ni_{80}Fe_{20}}(4.0)/\mathrm{Co_{90}Fe_{10}}(1.5)/\mathrm{Cu}(2.5)/\mathrm{Co_{90}Fe_{10}}(4.0)/\mathrm{Ir_{20}}$

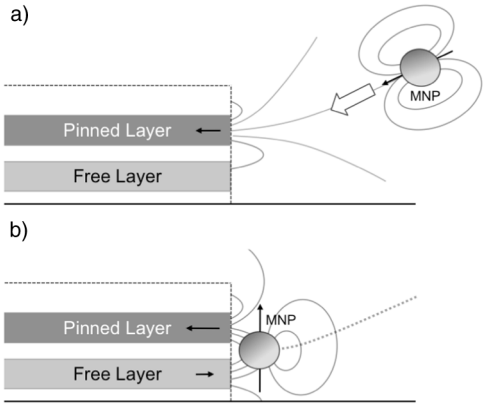

Fig. 1. Diagram of fringe-field capture and detection. (a) MNP capture, (b) increased coupling between layers due to presence of captured MNP.

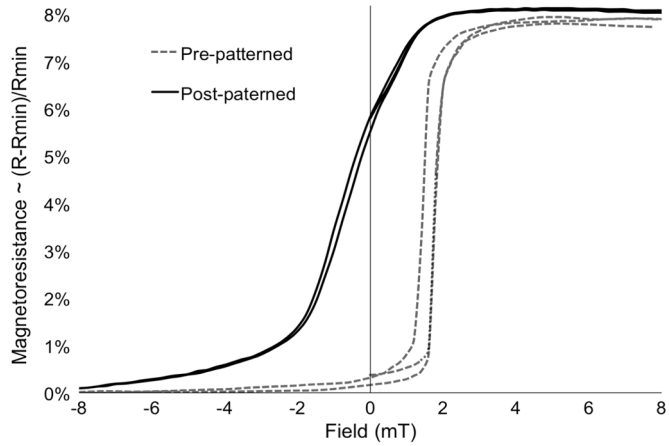

Fig. 2. Pre- and post-patterned MR measurements of optimized SV.

$\mathrm{Mn_{80}}(8.0)/\mathrm{Ta}(3.0)/\mathrm{Ru}(3)$, where the thickness of each layer is given parenthetically in nm. The Ni-Fe and Co-Fe layers together form the free layer of the SV; Cu serves as the spacing layer; Co-Fe, exchange biased by the Ir-Mn layer above, serves as the pinned layer. The stack design uses a thicker-than-typical pinned layer to increase the total magnetic moment of the layer, enhancing MNP trapping.

MR curves of the deposited pre-patterned SV material were measured from -10.0 to 10.0 mT with 4-point probes. Similar MR post-patterning curves where also recorded with 2-point probe measurements. Pre- and post-patterned MR curves of the optimized SV recipe can be seen in Fig. 2. Pre-patterning, the SV demonstrated a low zero-field resistance measurement. This means that the zero-field state of the pinned- and free layers is parallel alignment, indicating significant Néel coupling between the layers. Post-patterning, however, magnetostatic coupling from the edges of the SV balances out the Néel coupling yielding high sensitivity (dR/dH) at zero field. The thickness of the optimized spacing layer (2.5 nm) was tuned for a precise amount of magnetostatic coupling between pinned and free layers in post-patterned SVs. Sensitivity is maximized when free layer spins are oriented orthogonal to those in the pinned layer, which indicates a MR curve centered at zero field. The post-patterned measurement (Fig. 2) demonstrates such a MR curve. We would expect a similar field shift in the MR curve to occur when MNPs are present on the periphery of the patterned SVs, as their presence would effectively increase magnetostatic coupling between pinned and free layers.

B. Device Design and Fabrication

The integrated device, including GMR sensor and microfluidic channels, is constructed through μm-lithographic-based microfabrication. SV elements $(2 \times 200\ \mu\mathrm{m})$ are patterned with ion milling to a depth of 50 nm (penetrating $\sim$19 nm into the substrate). In the same process, a 10 nm passivation layer of silicon nitride $(\mathrm{Si_3N_4})$ is deposited to the edge of the SV to prevent corrosion of the exposed Fe-containing layers. SV elements are interconnected via Ti/Au/Ti electrical leads. The device surface is subsequently covered by an additional 20 nm thick layer of silicon nitride, leaving SV element edges and electrical contact pads exposed. The nitride layer makes the surface hydrophilic, reducing electrical contact with the liquid and enhancing adhesion with SU-8. SV elements, electrical leads, and nitride layer can be viewed in the SEM image of Fig. 3.

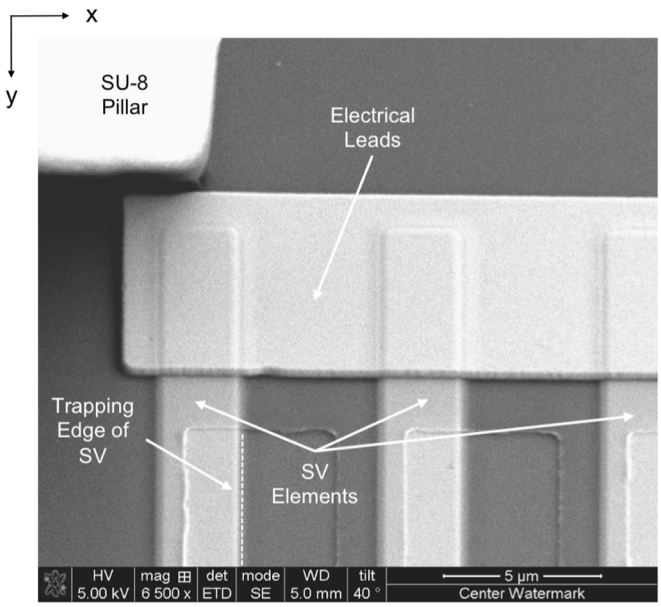

Fig. 3. SEM image of SV elements, electrical leads, silicon nitride layer, SU-8 pillar, and the exposed trapping edge in Array-1. Fluid and MNPs travel in the $(+\mathrm{y})$-direction, and external DC fields are applied along the x-direction. The width of the SV elements is 2 μm.

SV elements are electrically connected in sets of 31 electrically parallel strips; 15 of these sets are then arranged in electrical series to form the total SV array. The total device consists of four SV arrays arranged in a Wheatstone bridge circuit, seen in Fig. 4. All SV elements are physically in parallel alignment, and flow is parallel to the length of the SV elements. Two elements are in contact with sample (Cell 2) and the other two are in contact with reference liquid (Cells 1 and 3). The bridge circuit acts to minimize environmental noise, thermal, and dielectric signals.

Microfluidic channel walls were patterned with SU-8 (an epoxy-based negative photo-reactive polymer), and capped with polydimethylsiloxane (PDMS). Bonding between PDMS

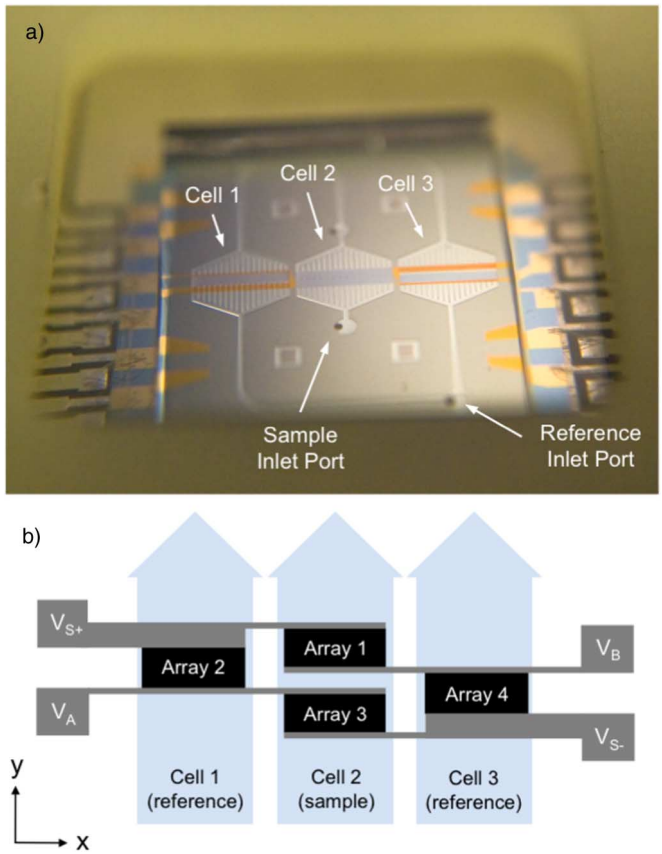

Fig. 4. (a) Image of fully assembled device showing fluid cells and inlet port. (b) Diagram of bridge circuit. Fluid and MNPs travel in the $(+\mathrm{y})$-direction, and external DC fields are applied along the x-direction.

and SU-8 was achieved through a process with nitrogen plasma was used where amino groups are produced on the surface of the PDMS and bonded with residual epoxy groups on the surface of the SU-8 [7]. Sample and reference liquids are injected through inlet ports originating on the back-side of the device, into microfluidic channels located on the front of the device. Inlet ports are created through a back-side aligned deep-RIE (reactive ion etch) process. SU-8 pillars support the PDMS ceiling in each cell. A portion of one of the SU-8 pillars can be seen in the SEM image in Fig. 3, directly preceding Array-1.

C. Sample Preparation and Procedure

MNP sample suspensions for testing the functionality of the device used Molday-ION MNPs from BioPAL (a commercial agent used for in vivo cell tracking)[1]. Molday-ION MNPs are iron oxide-based super-paramagnetic particles stated as having 30 nm nominal hydrodynamic diameter and 8 nm nominal magnetic core diameter. The starting suspension is diluted in reference liquid to a concentration of $1.2 \times 10^{10} \pm 4.0 \times 10^{9}\ \mathrm{MNP/mL}$ from an initial concentration of $1.6 \times 10^{15} \pm 5.0 \times 10^{14}\ \mathrm{MNP/mL}$. The initial concentration was estimated from the manufacturer's stated concentration of Fe (2 mg/mL) and nominal core diameter (8.5 $\pm$ 1.5 nm); and by assuming the MNPs to have a nominally spherical shape, and assuming a magnetite $(\mathrm{Fe_3O_4})$ core density of 5.175 g/mL [8]. The aforementioned reference liquid is a mixture of DI water and phosphate buffer tuned to a conductance of 100 $\mu\mathrm{S/cm}$. All samples and reference liquids were degassed directly before use. Sample and Reference liquids intended for measurement were flowed through Cell 2 at a rate of 5 $\mu\mathrm{L/min}$. Reference liquid was also injected into Cells 1 and 2 simultaneously at a rate of 5 $\mu\mathrm{L/min}$, however bridge voltage measurements showed that varying the reference liquid flow rate in Cells 1 and 2 had no noticeable effect on bridge voltage. Each measurement described in the following results resection were preformed under flow. Measurements consist of MR field sweeps as a function of bridge voltage vs. applied field from 10.0 to -10.0 mT (Sweep-1) and from -10.0 to 10.0 mT (Sweep-2).

[1]Certain commercial materials are identified to clarify experimental methods. Such identification does not imply recommendation or endorsement by the National Institute of Standards and Technology, nor does it imply that the materials identified are necessarily the best available for the purpose.

III. Results

Injections were performed as follows: 1) Reference liquid is injected and measured after $\sim$10 minutes of flow (Reference-1). 2) Sample is injected and measured after $\sim$10 minutes of flow (Sample-1). 3) Sample continues flowing for $\sim$16.6 hours followed by an injection of reference liquid and measured after $\sim$10 minutes of flow (Reference-2). 4) Reference continues flowing for $\sim$24.8 hours followed by an injection of sample and measured after $\sim$10 minutes of flow (Sample-2). 5) Sample is allowed to flow for $\sim$27.5 hours and a second measurement is taken after this period (Sample-3). 6) Reference liquid is injected and measured after $\sim$10 minutes of flow (Reference-3).

Fig. 5 and Fig. 6 show the MR responses for all reference and sample measurements. Fig. 5 shows the response for 10.0 to -10.0 mT, and Fig. 6 shows responses for -10.0 to 10.0 mT. The difference in MR response curves between Sweep-1 and -2 is likely the result of a minor hysteresis loop in the field cycling of the device. For comparison with measured responses, Reference-1 data were artificially shifted by 0.2 mT, and the resulting difference between shifted and non-shifted MR curves are plotted both in Fig. 5 and Fig. 6. The resulting difference curve is proportional to the gradient of the curve.

The field-shifted curves show a response similar to that of artificially shifted 0.2 mT field shift data. This indicates that the response of sample and reference are due to shifts in field, the predicted response due to MNP capture. Variations in the magnitude of $\mathrm{MR\ curve} \sim (\mathrm{(Vmax - Vmin)/Vmin})$ are also apparent, seen as variations in MR response at 8.0 mT in both Fig. 5 and Fig. 6. Variations in the magnitude of MR curves are ambiguous and could be a result of SV corrosion, a difference in conductance of the sample vs. reference liquid (possibly due to the presence of MNPs in suspension), or a magnetic response due to the presence of MNPs close to the surface of the SV. The MR responses of sample and reference measurements are consistent with partial and time dependent MNP capture. Difference in responses between Sample-2 and -3 measurements indicate a greater number of MNPs were captured during this interval. Additionally, we see little response from the Sample-1 measurement, which had a total exposure of $\sim$10 minutes, compared with Sample-2 and -3, which had an exposure of $\sim$27.5

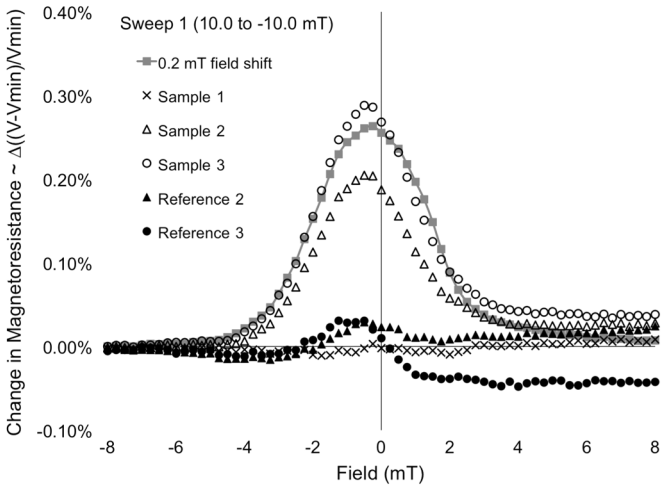

Fig. 5. Difference in MR curves from Reference-1 measurement in units of percent change in bridge voltage. Field sweep is from 10.0 to −10.0 mT. The observed shift is constant with a field shift of 0.2 mT in the Reference-1 measurement.

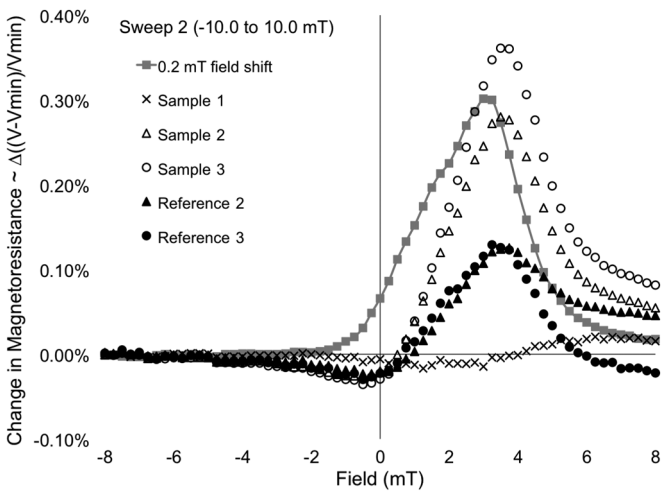

Fig. 6. Difference in MR curves from Reference-1 measurement in units of percent change in bridge voltage. Field sweep is from −10.0 to 10.0 mT. The observed shift is constant with a field shift of 0.2 mT in the Reference-1 measurement.

hours. The difference between sample and reference measurements indicates that some, but not all, MNPs are retained during switches between sample and reference liquids. Due to the small size of the MNPs, and their suspension in fluid, we cannot visually verify the trapping or retention of MNPs to the edge of SV.

IV. Conclusion

Our device has demonstrated a field shift response after exposure to suspension fluid containing MNPs. The observed field shift is consistent with the hypothesized increase in magnetostatic coupling between layers that can be attributed to the presence of MNPs on the edge of the SV elements. Sample-2 and -3 measurements are compatible with a field shift of ∼0.2 mT. Test of the response vs. concentration, and response vs. time of exposure, must still be performed to fully validate the capture and detection of MNPs. The device also requires further development to be suitable for industrial applications. During testing, the device showed high sensitivity to conductivity differences in sample and reference; when looking at the overall bridge voltage of the device, changes due to the presence of MNP are many orders of magnitude less then changes due to variations in the conductance. Despite this fact, we were able to isolate a signal indicative of MNP capture.

Acknowledgment

This work was supported in part via National Science Foundation award IIP 1024720 from the Industry/University Cooperative Research Center for Membrane Science, Engineering and Technology. Additional support was received from Department of Commerce Grant 70NANB10H02 as part of the Measurement Science and Engineering Research Training Fellowship.

References

[1] S. M. Thompson, "The discovery, development and future of GMR: The Nobel Prize 2007," *J. Phys. D: Appl. Phys.*, vol. 41, no. 9, p. 093001, May 2008.

[2] D. R. Baselt, G. U. Lee, M. Natesan, S. W. Metzger, P. E. Sheehan, and R. J. Colton, "A biosensor based on magnetoresistance technology," *Biosensors Bioelectron.*, vol. 13, no. 7–8, pp. 731–739, Oct. 1998.

[3] G. Li, S. Sun, R. J. Wilson, R. L. White, N. Pourmand, and S. X. Wang, "Spin valve sensors for ultrasensitive detection of superparamagnetic nanoparticles for biological applications," *Sens Actuators A Phys*, vol. 126, no. 1, pp. 98–106, 2006.

[4] W. R. Altman, J. Moreland, S. E. Russek, and V. M. Bright, "Optimization of spin-valve parameters for magnetic bead trapping and manipulation," *J. Magn. Magn. Mater.*, vol. 322, no. 21, pp. 3236–3239, Nov. 2010.

[5] E. Mirowski, J. Moreland, S. Russek, M. Donahue, and K. Hsieh, "Manipulation of magnetic particles by patterned arrays of magnetic spin-valve traps," *J. Magn. Magn. Mater.*, vol. 311, no. 1, pp. 401–404, Apr. 2007.

[6] R. L. Millen, J. Nordling, H. A. Bullen, M. D. Porter, M. Tondra, and M. C. Granger, "Giant magnetoresistive sensors. 2. Detection of biorecognition events at self-referencing and magnetically tagged arrays," *Analytical Chemistry*, vol. 80, no. 21, pp. 7940–7946, Nov. 2008.

[7] Z. Zhang, P. Zhao, G. Xiao, B. R. Watts, and C. Xu, "Sealing SU-8 microfluidic channels using PDMS," *Biomicrofluidics*, vol. 5, no. 4, pp. 046503–046503-8, Nov. 2011.

[8] J. W. Anthony, *Handbook of Mineralogy*. Tucson, AZ: Mineral Data Pub, 1995.